Modulation of Protein−Surface Interactions on Nanopatterned Polymer Films

K. H. Aaron Lau, Joona Bang, Craig J. Hawker, Dong Ha Kim,* and Wolfgang Knoll*

Max Planck Institute for Polymer Research, Ackermannweg 10, D-55128 Mainz, Germany, Department of Chemical and Biological Engineering, Korea University, Seoul 136-701, Republic of Korea, Materials Research Laboratory, University of California at Santa Barbara, Santa Barbara, California 93106, and Department of Chemistry and Nano Science, Ewha Womans University, Seoul 120-750, Republic of Korea

Received October 13, 2008; Revised Manuscript Received January 30, 2009

The introduction of nanoscale features brings with it a high density of surface interface boundaries and effectively introduces an additional boundary material that exhibits properties different from the surrounding surfaces. We systematically varied the feature size of self-assembled polystyrene-*block*-poly(methyl methacrylate) copolymer nanopatterns from 13 to 200 nm and demonstrated that the basic property of protein adsorption on a nanopatterned surface can be modulated by the length density of surface interfaces present. Protein adsorption on the nanopatterns could be described by a modified adsorption affinity along the surface interface with an effective width on the length-scale of individual proteins. Due to the intrinsic high density of surface interfaces in many polymeric thin film nanopatterns and structures, the interaction of proteins with such interfaces may be of particular relevance to cell−surface studies and to biomaterial and biosensor applications involving nanoscale features.

Introduction

The ability to define surface structures on the nanoscale has the potential to significantly advance the fields of biosensing, biomaterials, and cell−surface studies. Nanoarrays of biomolecular elements are important for high-throughput biosensing.[1−3] Cell−surface studies with nanopatterns of biochemical or topographic cues may offer mechanistic insights into biochemical pathways that regulate cell−surface interactions,[2,4−6] and provide knowledge for designing biomaterials that mimic the biological system.[7,8] The introduction of nanoscale features brings with it a high density of surface interface boundaries and effectively introduces an additional interface material that may exhibit properties different from the surrounding surfaces. Investigation of protein interactions with these interfaces may inform the design of protein-based biosensors and, because adsorbed proteins mediate the interaction of cells with a surface,[4,9,10] complement our understanding of cell−surface interactions.

Protein adsorption on micro- and nanopatterns has been an active area of investigation, especially in relation to developing protein patterning techniques for array sensing applications.[11−17] Previous reports have also explored the effect of a nanopattern on adsorption behavior. For example, the presence of chemical nanostripes with line widths close to that of individual proteins has been shown to induce proteins to preferentially adsorb with an orientation aligned with the nanopattern's anisotropy.[3,18] Also, the amount of proteins adsorbed on the nanostructured surface of a homogeneous material was observed to increase with increasing feature density and nanoscale roughness.[19] Moreover, the presence of nanostructures on a surface has been shown to enhance the activity of an adsorbed protein.[20] Recently, based on ex situ AFM measurements, an enhanced protein adsorption affinity along surface interfaces of polymer patterns has been proposed.[21] However, the influence of hydrodynamic shear forces, induced during sample rinsing, on the spatial distribution of proteins adsorbed on a patterned surface,[17] complicates the interpretation of the results.

In this contribution we demonstrate that the basic property of protein adsorption on a nanopatterned surface can be significantly modified by the density of surface interfaces present. A range of polystyrene-*block*-poly(methyl methacrylate) (PS-*b*-PMMA) copolymer nanopatterned surfaces were prepared,[22−24] and the density of surface interfaces systematically varied by more than an order of magnitude. Significantly, the nanopattern with the highest interface density exhibited pattern domains with dimensions corresponding to individual proteins, and these surfaces were topographically flat relative to the dimensions of proteins. To these tailored two-dimensional nanopatterned surfaces, the adsorption of immunoglobulin-G (IgG) was investigated and compared to the adsorption on PS and PMMA surfaces lacking interfaces. The nanopatterns were characterized with atomic force microscopy (AFM), and the corresponding protein adsorption was monitored in situ by surface plasmon resonance spectroscopy (SPR). PS and PMMA have almost identical surface energies in air,[25−27] thus skin layer formation was minimized during PS-*b*-PMMA block copolymer self-assembly, and topographically flat polymer nanopatterned surfaces could be prepared.[17,24,25] The use of an in situ technique for quantifying protein adsorption ensured that the measurements reflected the native configurations of the proteins adsorbed on the nanopatterned surfaces. Moreover, unlike previous studies that employed an extreme contrast in hydrophobicity to generate a biomolecular response, such as with alkyl/poly(ethylene-oxide)[3,18] or oxide/metal[20] nanopatterns, the PS and PMMA used in this report are both poorly solvated in water and are comparatively similar in hydrophobicity.[28−30] Thus, the present results on PS-*b*-PMMA nanopatterns put an emphasis on the presence of surface chemical interfaces, in addition to a difference in chemistry across the interfaces.

* To whom correspondence should be addressed. E-mail: dhkim@ewha.ac.kr (D.H.K.); knoll@mpip-mainz.mpg.de (W.K.).

10.1021/bm801158x CCC: $40.75
Published on Web 03/20/2009

Experimental Section

Materials. PS-*b*-PMMA with PS/PMMA block number molecular weights (M_n, in kg/mol) of 20.2/50.5, 26.4/68, 106/99, and 868/857 and polydispersities of 1.07, 1.18, 1.09, and 1.3, respectively, were purchased from Polymer Source Inc., Dorval, Canada, and used as received. The PS-*b*-PMMA with M_n of PS/PMMA = 21.5/20.6 and 35.7/35.9 and polydispersities of 1.07 and 1.09, respectively, were synthesized by living anionic polymerization. The cross-linkable, random copolymer of styrene, methyl methacrylate, and reactive benzocyclobutene (BCB) (P(S-r-BCB-r-MMA)), with M_n = 25 kg/mol, and polydispersity = 1.18, used to prepare the neutral surface energy layer, was synthesized by living free-radical polymerization. The syntheses of the polymers have been described elsewhere.[24] Polished LaSFN9 high refractive index glass substrates were purchased from Hellma Optik, Germany. Phosphate buffered saline (PBS; 10 mM phosphate buffer, 2.7 mM KCl and 137 mM NaCl, pH 7.4 (25 °C)) was purchased from Sigma-Aldrich, Germany. Affinity purified whole goat antirabbit IgG (biotinylated) was purchased also from Sigma-Aldrich. Affinity purified whole mouse antigoat IgG was purchased from Pierce Biotechnology, U.S.A. Protein concentrations were verified by UV absorbance assay (measured using a BioPhotometer, Eppendorf, Germany).

Preparation of Copolymer Thin Film Templates. PS-*b*-PMMA nanopatterns were prepared on gold-coated glass substrates with a ~10 nm thick P(S-r-BCB-r-MMA) "neutral surface energy" layer according to a reported method.[24] Briefly, first the 0.3 wt % P(S-r-BCB-r-MMA) solutions in benzene were spin-coated at 3000 rpm onto the gold-coated substrates and cross-linked in vacuum (220 °C) overnight. Then PS-*b*-PMMA films were spin-coated onto the functionalized substrates from solutions in toluene. The concentrations and spin speeds used ranged from 1 to 2.5 wt % and from 1800 to 4500 rpm, respectively, to achieve copolymer layer thicknesses of 25, 25, 30, 30, 51, and 64 nm (measured by profilometer P-10, KLA Tencor, U.S.A.), for copolymers of M_n = 20.2/50.5, 26.4/68, 21.5/20.6, 35.7/35.9, 106/99, and 868/857 kg/mol, respectively. Samples corresponding to the first four of these copolymers were then annealed in vacuum at 180 °C for 2 days, and samples of the last two copolymers were annealed at 200 °C for 2 days. Finally, the samples were rinsed in ethanol and then in deionized water before use. Gold layers (50 nm) were coated on the glass substrates by thermal evaporation; a 2 nm Cr adhesion layer was also used (Autolab 306, BOC Edwards, UK).

Atomic Force Microscopy (AFM) and Computer Image Analysis. AFM was performed with a Nanoscope IIIa Multimode (Digital Instruments/Veeco Metrology, U.S.A.). Two types of tetrahedral silicon micro cantilevers (Olympus, Japan) were used: 42 N/m, 300 kHz tips for general PS-*b*-PMMA characterization; and 1.8 N/m, 70 kHz tips for surfaces decorated with proteins. The tip radius was specified by the manufacturer to be <7 nm. The PS-*b*-PMMA domain center-to-center distances (λ_{C-C}) were determined from maxima in the 2D frequency transforms of AFM phase images. Identification of the PS and PMMA domains appearing in AFM phase images was accomplished by cluster thresholding of the histogram[31] to distinguish between dark and light phases in the images corresponding to the respective domains. The characteristic PS domain widths (d_{PS}), surface fractions (f_{PS}), and domain interface length densities (l_{interf}) were then measured from the identified nanopatterns with the help of the particle analysis tool found in the image analysis software ImageJ.[32] See Supporting Information for details on the thresholding procedure and on calculating d_{PS}, f_{PS}, and l_{interf}.

Surface Plasmon Resonance (SPR). In situ SPR experiments were performed on a purpose-built system.[33,34] Surface plasmons were excited at the resonance angle (θ_r) and measured as a sharp minimum in intensity, as a laser (632.8 nm) was reflected off the gold−glass interface of the gold-coated glass substrates over a range of incidence angles under total internal reflection. Protein adsorption was observed as a shift in θ_r, and this was related to protein layer thickness by Fresnel calculations[33] using an IgG layer refractive index = 1.53 (dry mass value).[35] The mass density of protein adsorbed was then calculated from the optical thickness by de Feijter's formula using a protein refractive index increment of 0.182 cm^3/g.[35] A Teflon liquid cell (internal dimensions: 6 mm deep; 3.5 mm in radius) was clamped onto the samples and was used in conjunction with the SPR setup to exchange protein solutions and rinsing buffers in situ. Exchange of the liquid cell content was accomplished by direct injection and extraction of the liquid content via separate syringe needles. Water surface tension and the wetting of the sample surface ensured that the sample surface was always wetted during syringe action (PS and PMMA are less hydrophobic than the Teflon). Full exchange of the liquid contents was ensured by repeating the syringe exchange three times during injection of protein solutions and five times during buffer rinsing. The syringe exchange was found to be more effective than using a pump-operated flow cell with either (i) a thin cross section of the liquid flow path, which enabled laminar flow within the cell and complete exchange of the flow cell contents, but which also induced significant hydrodynamic shear forces on the sample surface, or (ii) a large cell volume, which did not support proper exchange of cell contents.

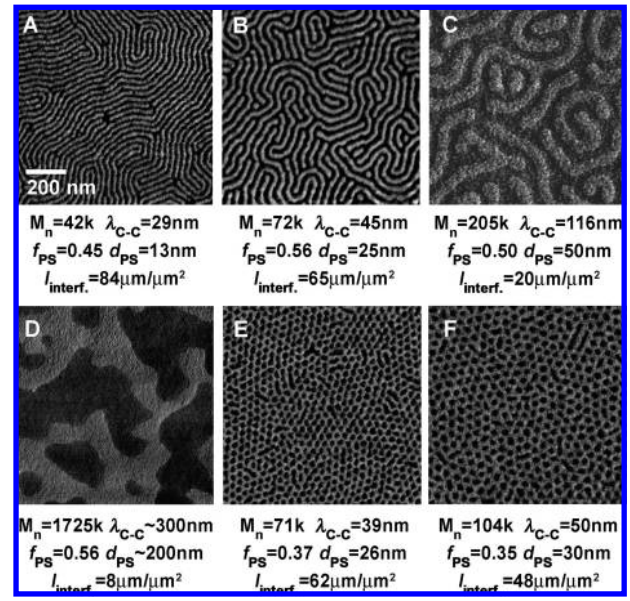

Figure 1. AFM phase images of PS-*b*-PMMA nanopatterns (1 × 1 μm^2, 20° phase scale). PS domains are indicated as darker areas than PMMA areas. (A−D) Alternating PS and PMMA striped domains. (E−F) PS dot arrays with local hexagonal ordering. The corresponding total molecular weight (M_n, in g/mol), l_{interf}, d_{PS}, and f_{PS} are also shown. Although a high M_n for (D) prevented long-range self-assembly, the sample showed characteristic averaged values of λ_{C-C} and l_{interf} (calculated from measurements spanning 5 × 5 μm^2).

Results and Discussion

AFM phase measurements of the nanopatterned PS-*b*-PMMA thin films are shown in Figure 1. PS surfaces were revealed as dark regions with a phase shift smaller than for the light PMMA regions.[36,37] Alternating stripes of PS and PMMA (Figure 1A−D) and hexagonally ordered PS domains arrayed in a PMMA matrix (Figure 1E,F) resulted, respectively, from PS-*b*-PMMA self-assembly into lamella and cylindrical morphologies oriented normal to the surface.[22−24] The periodic domain center-to-center distance (λ_{C-C}) was varied over an order of magnitude from 29 to ~300 nm, corresponding to characteristic PS domain widths (d_{PS}) of 13 to ~200 nm. The nanopatterns were also characterized by the PS surface fraction (f_{PS}), and the length density of surface interfaces delineating nanopatterned surfaces (l_{interf}). As the domain feature density increased, l_{interf}

increased from 8 to 84 $\mu m/\mu m^2$. The maximum height variation (R_{max}) across any 1 × 1 μm^2 surface for nanopatterns with λ_{C-C} < 100 nm was <1 nm, and the maximum local curvature for all samples was <0.1 nm^{-1} (see Supporting Information). Therefore, the variation in topography across the PS/PMMA interfaces was significantly smaller than the dimensions of the proteins used (IgG: 14 × 9 × 4 nm^3)[38,39] and the nanopatterned surfaces were considered flat. Note that, although limited PMMA chain mobility at the solid−water interface over time-scales of many hours has been demonstrated,[40] PMMA is only poorly solvated in water and PS is even less so.[41] Therefore, any PS-*b*-PMMA swelling is not expected to alter the relative flatness of the PS-*b*-PMMA nanopatterns with respect to the dimensions of the protein. Note also that, due to the flat topography of the chemical nanopatterns, tip convolution on the measurements of the geometric parameters of the nanopatterns was minimal.

In situ SPR results of adsorption on the nanopatterns from 17 μg/mL IgG in PBS are shown in Figure 2. Two kinds of IgG, mouse antigoat (MxG) and goat antirabbit (GxR), were used to cross-verify the results. As an example, Figure 2A compares the kinetics of GxR−IgG adsorption on a hexagonally arrayed PS domain nanopattern (Figure 1F), with adsorption on pure PS and pure PMMA surfaces. In general, the amount of IgG adsorbed on PS (Γ_{PS}) is higher than that on PMMA (Γ_{PMMA}).[28,42] Because the nanopatterned surface consists of both PS and PMMA domains, one might expect the amount of IgG adsorbed to be the surface fraction weighted average of Γ_{PS} and Γ_{PMMA}, that is, the linear additive rule, with the presumed adsorbed amount $\Gamma' = f_{PS}\Gamma_{PS} + (1 - f_{PS})\Gamma_{PMMA}$. However, the measured IgG adsorption on PS-*b*-PMMA ($\Gamma_{PS\text{-}b\text{-}PMMA}$) was found to be significantly higher than Γ' (Figure 2A). Furthermore, this anomaly was observed, to different degrees, for all the nanopatterns and IgG's. Normalizing $\Gamma_{PS\text{-}b\text{-}PMMA}$ by Γ' gives Γ_{norm}, which characterizes the "excess" protein adsorbed (values taken to be the adsorbed amount at 180 min). Γ_{norm} is plotted against λ_{C-C} in Figure 2B, and a dramatic enhancement in the amount of protein adsorbed is seen as λ_{C-C} decreased and approached the dimensions of an individual IgG (14 × 9 × 4 nm^3).[38,39] On the other hand, no relationship could be discerned between Γ_{norm} and f_{PS}. Interestingly, the nanopattern morphology also did not appear to influence the trend in Γ_{norm}. Analyzing the data subsets corresponding to the striped and the dot arrayed nanopatterns did not reveal significantly different trends. However, Figure 2C suggests a straightforward interpretation of the enhancement effect by plotting Γ_{norm} against l_{interf} for all samples. It shows that the observed increase in protein adsorption is directly related to the length of PS/PMMA surface interfaces present. Furthermore, because the amount of proteins adsorbed was observed to be enhanced on the nanopatterned PS-*b*-PMMA surfaces relative to equivalent areas of pure PS and PMMA surfaces, therefore, the PS/PMMA surface interface regions on the PS-*b*-PMMA nanopatterns may also be expected to have not an averaged adsorption behavior between these two constituent bulk materials, but an enhanced adsorption affinity.

In the present analysis, there is an uncertainty associated with the measurement of f_{PS} based on image analysis of the PS-b-PMMA nanopatterns which may be biased depending on the image thresholding technique used.[43] Indeed, since $\Gamma_{PS} > \Gamma_{PMMA}$, an underestimation of f_{PS} might lead to an apparent excess of proteins adsorbed on the nanopatterned surfaces. Nonetheless, the estimated uncertainty in f_{PS} in our experiments is far lower than would be required to explain the observed results shown in Figure 2. For example, for adsorption on the smallest nanopattern corresponding to Figure 1A, f_{PS} would have to be adjusted upward from the measured value of 0.43 to a hypothetical value of 0.81 to negate the measured ~25% increase in proteins adsorbed. Such a drastic discrepancy in f_{PS} was not observed by, for example, visual examination of the AFM image. Furthermore, no systematic under- or overestimation of f_{PS} measured relative to the volume fractions of the block copolymers used was found. Therefore, we believe our measurements of f_{PS} and of Γ_{norm} were valid, and the error bars in Figure 2B,C, which span four standard deviations (±2 SD), serve to underscore the certainty of the interface effect.

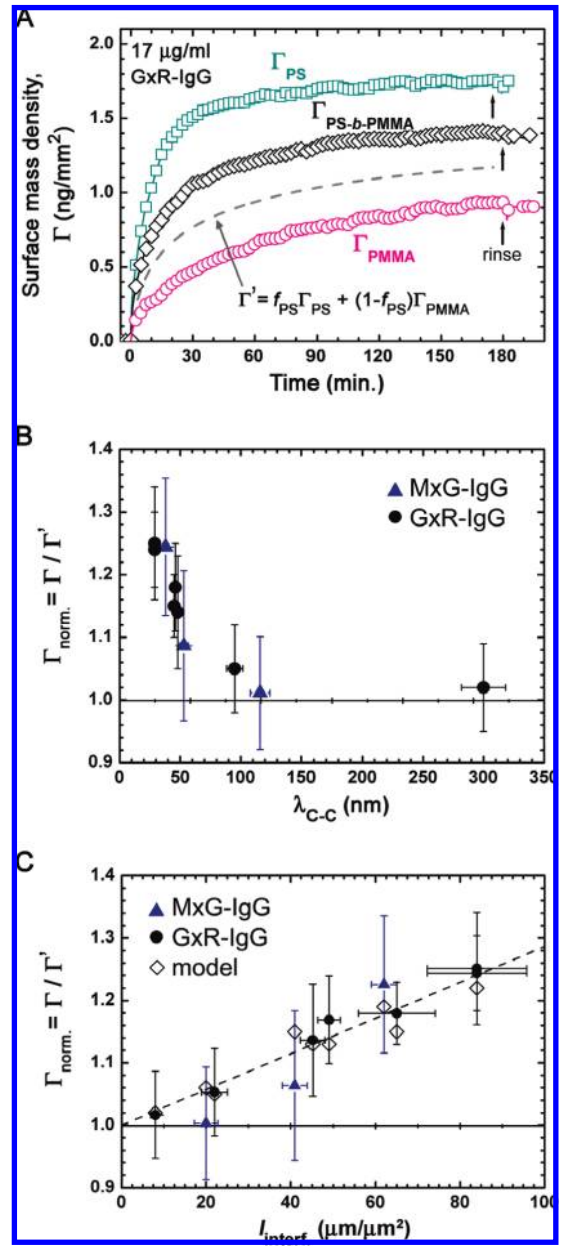

Figure 2. (A) G × R-IgG adsorption on PS, PMMA, and the PS-*b*-PMMA nanopattern corresponding to Figure 1F. The dashed line shows the hypothetical amount of IgG adsorbed calculated from the f_{PS} weighted-average of Γ_{PS} and Γ_{PMMA}. Short arrows indicate rinsing with PBS. (B) and (C) Γ_{norm} after 180 min adsorption, plotted against λ_{C-C} and l_{interf}, respectively. Open symbols in (C) show Γ_{norm} modeled using eq 1B with $\Gamma_{interf} = 1.67\ \Gamma_{PS}$ and $d_{interf} = 2$ nm. The dashed line is for guiding the eye only. The error bars show ± 2 SD.

The observed adsorption behavior may be described by a two-variable model that sums the amount of proteins separately adsorbed on the PS, the PMMA, and the interface surface regions

$$\Gamma_{norm} = \frac{1}{\Gamma'}\left(l_{interf}d_{interf}\Gamma_{interf} + \left(f_{PS} - \frac{l_{interf}d_{interf}}{2}\right)\Gamma_{PS} + \left(f_{PMMA} - \frac{l_{interf}d_{interf}}{2}\right)\Gamma_{PMMA}\right) \quad (1A)$$

$$= 1 + l_{interf}d_{interf}\left(\frac{\Gamma_{interf}}{\Gamma'} - \frac{\Gamma_{PS} + \Gamma_{PMMA}}{2\Gamma'}\right) \quad (1B)$$

where d_{interf} is the effective width and Γ_{interf} is the adsorption affinity of the PS/PMMA surface interface. The remaining terms have already been measured either by AFM (l_{interf}, f_{PS}, $f_{PMMA} = 1-f_{PS}$) or by SPR (Γ_{PS}, Γ_{PMMA}, and Γ').

Equation 1A shows explicitly how the normalized amounts of adsorbed protein on the different nanopattern domains are accounted for. In the first term, $l_{interf}d_{interf}$ defines the per unit surface area belonging to the interface region, and this product times Γ_{interf} is the amount of proteins adsorbed along the interfaces. The second and third terms describe the amounts of protein adsorbed on the PS and PMMA surfaces, respectively. Because the interface is now considered to have a finite width, d_{interf}, the surface fractions occupied by the two polymer components are reduced by the interface width. It is assumed that the interface extends into both the PS and PMMA domains equally. Therefore, the amounts of proteins adsorbed on the pure polymer surfaces are Γ_i times ($f_i - l_{interf}d_{interf}/2$) (where *i* stands for either PS or PMMA).

Figure 2C indicates that l_{interf} is the independent variable in the analysis, and eq 1A can be re-expressed as eq 1B to show this explicitly. Moreover, eq 1B expresses the conditions for which an interface effect may be expected ($\Gamma_{norm} \neq 1$): (i) if $d_{interf} > 0$ and (ii) if the interface possesses an adsorption affinity that is different from the average of the materials across the interface ($\Gamma_{interf} \neq (\Gamma_{PS} + \Gamma_{PMMA})/2$). Therefore, the fact that the data exhibits a positive slope in Figure 2C implies that the interface of the PS-*b*-PMMA nanopatterns has a finite width and that the interface's affinity for IgG adsorption is higher than the average of Γ_{PS} and Γ_{PMMA}. However, because d_{interf} and Γ_{interf} only appear as a product in eqs 1A and 1B, it is not possible to independently determine both values from fitting of the data. Nonetheless, a few limiting cases may be considered. First, it is plausible that the interface should have a width that is equal to or larger than the diameter of the PS-*b*-PMMA chain. Assuming a value of $d_{interf} = 0.8$ nm, that is, equal to the van der Waals chain diameter of PMMA,[40] an upperbound estimate of Γ_{interf} may be obtained: $\Gamma_{interf} = 3.2\Gamma_{PS} = 7.4\Gamma_{PMMA}$. In comparison, adsorption experiments on a homogeneous random copolymer surface with styrene and methyl methacrylate monomers mixed on the molecular scale in a 58:42 ratio showed an IgG adsorption affinity, $\Gamma_{P(S\text{-}r\text{-}MMA)}$, that equaled $1.2\Gamma_{PS}$ and $2.8\Gamma_{PMMA}$ (see Supporting Information). Assuming that $\Gamma_{interf} = \Gamma_{P(S\text{-}r\text{-}MMA)}$, fitting of the data gave $d_{interf} = 4.2$ nm. At the other extreme, by assuming Γ_{interf} to be marginally larger than the average [(Γ_{PS}, Γ_{PMMA})/2] fitting gave an unphysical value of $d_{interf} = 32$ nm, which is larger than the pattern periodicity of the smallest nanopattern $\lambda_{C-C} = 29$ nm. Assumed values of d_{interf} larger than the nanometer scale also led to lower tightness of fit with the data. Therefore, we believe that the observed enhancement in the amount of proteins adsorbed along the interface may best be described by $d_{interf} \sim 1$ nm and Γ_{interf} that is slightly higher than Γ_{PS}.

A differentiated affinity for protein adsorption along surface interfaces of nanopatterns may have possible contributions from the surface chemistry, and the packing geometry and orientation of the adsorbed proteins. First, surface interfaces are seldom atomically sharp and an IgG spanning the PS/PMMA interface has the possibility to interact with both PS and PMMA surfaces as well as a range of surface chemistries spanning between PS and PMMA. In the case of block copolymer surfaces, the differences in chain configurations along domain interfaces[22,44,45] (combined with any surface swelling effects) may contribute to the differentiation of the interface properties relative to surface bulk properties of either PS or PMMA. Therefore, the fact that a protein may span a chemically variable interface region may allow the residues of a protein to form attachment points[46] with different regions of the interface and make up, in the case of IgG, a more favorable overall physical interaction. The unique conformational state of the block copolymer interface between PS and PMMA domains[22,44] may also contribute to a nonaverage surface chemistry at that location. Second, the jamming limit to protein adsorption,[47] which defines the highest surface coverage of adsorbed proteins that can be randomly positioned on a surface (i.e., the effective full surface coverage of an adsorbed monolayer), may be higher at the interface between two surfaces with different rates of adsorption. In the present experiment, the lower adsorbed protein density on PMMA relative to that on PS effectively decreases the protein density along the PS side of the PS/PMMA interface, thus increases the number of adsorption sites on the interface large enough to accommodate further adsorption. Furthermore, the preferred orientation of the adsorbed proteins may also be influenced by a difference in surface chemistry, which may lead to modifications of the maximum surface mass density representing effective full surface coverage (monolayer coverage). The surface area occupied by an adsorbed IgG is 123 nm^2 if the protein is adsorbed "flat" with its longest axis parallel to the surface and 34 nm^2 if the IgG is adsorbed "standing" with its shortest axis parallel to the surface.[48] On a surface with highly favorable hydrophobic interactions, such as PS, a protein may adsorb preferentially flat (i.e., spread) on the surface to maximize the protein-surface interactions.[49] Higher degrees of spreading (i.e., a larger surface area occupied per adsorbed IgG) imply lower maxima for the mass density of a full protein monolayer, and "flat" and "standing" close-packed IgG monolayers correspond to surface mass densities of 2.2 and 7.8 ng/mm^2, respectively. In other words, the adsorbed mass density at any particular surface coverage may vary significantly depending on the adsorbed orientation of the irregularly shaped proteins. Furthermore, given the effect of geometric jamming mentioned above, the full monolayer mass densities are reduced to effective maxima corresponding to the jamming surface coverage. Therefore, the final amount of IgG adsorbed on PS (1.8 ng/mm^2; Figure 2A), which corresponds to a value slightly lower than a close-packed "flat" monolayer, may indicate an effective monolayer of IgG adsorbed predominantly in the "flat" configuration. This interpretation would also be consistent with the presence of a strong IgG-PS surface interaction.[49] On PMMA, the amount of IgG adsorbed was quite low compared with the theoretical maximum regardless of the adsorbed orientation. Because our SPR measurements indicated that the adsorbed amount along the interface was possibly higher than even on PS and that the surface coverage on PS might already correspond to an effective full monolayer, our results may suggest that more IgG were adsorbed in a "standing" orientation along the interface than on PS.

In terms of dynamics, protein−surface interactions during the initial adsorption may be expected to proceed close to equilibrium in our experiments, because of the relatively low protein

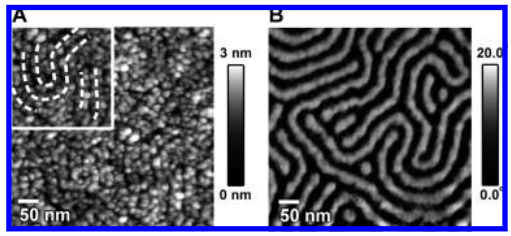

Figure 3. (A) AFM height image of a PS-*b*-PMMA block copolymer surface after 3 h G × R-IgG adsorption and rinsing with PBS. The AFM phase image of the original copolymer surface used is shown in (B), which is a partial, magnified view of Figure 1B. The inset in (A) sketches out the underlying PS-*b*-PMMA striped pattern in the lower right portion of the main image, inferred from the differences in protein densities observed.

concentration used and because the protein solution was not disturbed by hydrodynamic shear during the adsorption (see Experimental Section). If the arrival of adsorbing proteins was significantly increased, such as at higher protein concentrations, adsorbed proteins might not have enough time to reach their equilibrium conformations before nearby surfaces became occupied by additional protein adsorption. If the enhanced adsorption along the interface resulted primarily from differences in the adsorbed orientation/conformation, then at higher concentrations, the contrast in adsorption affinity between the PS and interface surfaces would decrease and the enhancement effect would be diminished. Further experiments are underway to explore this concentration effect.

The contrast between Γ_{interf}, Γ_{PS}, and Γ_{PMMA} may also be inferred from AFM measurements of the protein-covered PS-*b*-PMMA surface after adsorption. Figure 3A shows the AFM height image of the IgG covered block copolymer surface with $\lambda_{C-C} = 45$ nm and $d_{PS} = 25$ nm (Figures 1B and 3B). The image was taken after 3 h GxR-IgG adsorption. It can be seen that, although the entire surface was saturated with particulates ~10 nm in size, likely representing individual IgGs, the underlying chemical nanopattern of the microphase separated PS-*b*-PMMA could still be discerned due to differences in adsorbed protein density on the PS, PMMA, and interface regions. Due to the high protein coverage and the parity in dimensions of the IgG and the AFM tip radius, tip convolution prevented a precise determination of the surface coverage based on AFM data. Also, due to the high protein coverage and the uneven surface presented by the protein layer, high resolution in situ liquid AFM images of the sample in buffer could not be obtained. On the other hand, Figure 3A shows a topography variation <3 nm, which is less than the shortest axis of the IgG, and no multilayers or protein aggregates could be observed. Moreover, as discussed earlier, the SPR measurements indicated that the adsorbed mass density of proteins was no higher than for an effective monolayer of IgG adsorbed "flat" on the nanopatterns. Thus, all the proteins seen in Figure 3A were actually adsorbed directly on the nanopatterned polymer surface. Therefore, Figure 3A shows that multiply defined nanoregions of contrasting protein densities, with interface regions having a higher density than possible with the constituent pure phase materials, may be tailored from the nanoscale juxtaposition of PS and PMMA block copolymer domains.

Conclusions

This contribution demonstrates that protein adsorption on topographically flat, chemically heterogeneous nanopatterned polymer surfaces can be modulated by the length density of surface interfaces delineating the nanopatterns. Periodic nanopatterns spanning an order of magnitude in feature size and interface density were obtained by PS-*b*-PMMA self-assembly, and protein adsorption on the nanopatterns could be described by an enhanced adsorption affinity along the interface. Importantly, adsorption along the PS/PMMA interface was found not to be an average of the adsorption behavior on PS and PMMA surfaces, but to be enhanced with respect to both types of polymer surfaces. This interface effect was also found not to depend on other nanopattern parameters such as the pattern morphology. Due to the intrinsic high density of surface interfaces in polymeric thin film nanopatterns and structures, the interaction of proteins with such interfaces may be of particular relevance to cell−surface studies and to biomaterial and biosensor applications involving nanoscale features.

Acknowledgment. This work was supported by the Korea Science and Engineering Foundation (KOSEF) grant funded by the Korea government (MEST; No. R11-2005-008-00000-0; R01-2008-000-11712-0) and by the Seoul Research and Business Development Program (10816). We are indebted to J. T. Goldbach for the synthesis of the block copolymers with symmetric composition.

Supporting Information Available. AFM height images corresponding to Figure 1, lateral force measurements of the PS-*b*-PMMA surface compositions, full SPR data corresponding to Figure 2, and an explanation on the image analysis used for obtaining the nanopattern parameters. This material is available free of charge via the Internet at http://pubs.acs.org.

References and Notes

(1) Lee, K. B.; Park, S. J.; Mirkin, C. A.; Smith, J. C.; Mrksich, M. *Science* **2002**, *295*, 1702–1705.
(2) Lee, K. B.; Kim, E. Y.; Mirkin, C. A.; Wolinsky, S. M. *Nano Lett.* **2004**, *4*, 1869–1872.
(3) Pallandre, A.; De Meersman, B.; Blondeau, F.; Nysten, B.; Jonas, A. M. *J. Am. Chem. Soc.* **2005**, *127*, 4320–4325.
(4) Arnold, M.; Cavalcanti-Adam, E. A.; Glass, R.; Blummel, J.; Eck, W.; Kantlehner, M.; Kessler, H.; Spatz, J. P. *ChemPhysChem* **2004**, *5*, 383–388.
(5) Agheli, H.; Malmstrom, J.; Larsson, E. M.; Textor, M.; Sutherland, D. S. *Nano Lett.* **2006**, *6*, 1165–1171.
(6) Senaratne, W.; Sengupta, P.; Jakubek, V.; Holowka, D.; Ober, C. K.; Baird, B. *J. Am. Chem. Soc.* **2006**, *128*, 5594–5595.
(7) Park, H.; Cannizzaro, C.; Vunjak-Novakovic, G.; Langer, R.; Vacanti, C. A.; Farokhzad, O. C. *Tissue Eng.* **2007**, *13*, 1867–1877.
(8) Engel, E.; Michiardi, A.; Navarro, M.; Lacroix, D.; Planell, J. A. *Trends Biotechnol.* **2007**, *26*, 39–47.
(9) Mrksich, M. *Curr. Opin. Chem. Biol.* **2002**, *6*, 794–797.
(10) Stevens, M. M.; George, J. H. *Science* **2005**, *310*, 1135–1138.
(11) Neto, C. *Phys. Chem. Chem. Phys.* **2007**, *9*, 149–155.
(12) Li, L.; Hitchcock, A. P.; Robar, N.; Cornelius, R.; Brash, J. L.; Scholl, A.; Doran, A. *J. Phys. Chem. B* **2006**, *110*, 16763–16773.
(13) Morin, C.; Hitchcock, A. R.; Cornelius, R. M.; Brash, J. L.; Urquhart, S. G.; Scholl, A.; Doran, A. *J. Electron Spectrosc. Relat. Phenom.* **2004**, *137−40*, 785–794.
(14) Kumar, N.; Hahm, J. I. *Langmuir* **2005**, *21*, 6652–6655.
(15) Kumar, N.; Parajuli, O.; Hahm, J. *J. Phys. Chem. B* **2007**, *111*, 4581–4587.
(16) Parajuli, O.; Gupta, A.; Kumar, N.; Hahm, J.-i. *J. Phys. Chem. B* **2007**, *111*, 14022–14027.
(17) Lau, K. H. A.; Bang, J.; Kim, D. H.; Knoll, W. *Adv. Funct. Mater.* **2008**, *18*, 3148–3157.
(18) Denis, F. A.; Pallandre, A.; Nysten, B.; Jonas, A. M.; Dupont-Gillain, C. C. *Small* **2005**, *1*, 984–991.
(19) Riedel, M.; Müller, B.; Wintermantel, E. *Biomaterials* **2001**, *22*, 2307–2316.
(20) Sutherland, D. S.; Broberg, M.; Nygren, H.; Kasemo, B. *Macromol. Biosci.* **2001**, *1*, 270–273.
(21) Kumar, N.; Parajuli, O.; Gupta, A.; Hahm, J.-i. *Langmuir* **2008**, *24*, 2688–2694.

(22) Fasolka, M. J.; Mayes, A. M. *Annu. Rev. Mater. Res.* **2001**, *31*, 323–355.
(23) Hamley, I. W. *Nanotechnology* **2003**, *14*, R39−R54.
(24) Ryu, D. Y.; Shin, K.; Drockenmuller, E.; Hawker, C. J.; Russell, T. P. *Science* **2005**, *308*, 236–239.
(25) Kim, H.-C.; Russell, T. P. *J. Polym. Sci., Part B: Polym. Phys.* **2001**, *39*, 663–668.
(26) Schrader, D. In *Polymer Handbook*, 4th ed.; Brandrup, J., Immergut, E. H., Grulke, E. A., Abe, A., Bloch, D. R., Eds.; Wiley: New York, 1999; p V/91.
(27) Wunderlich, W. In *Polymer Handbook*, 4th ed.; Brandrup, J., Immergut, E. H., Grulke, E. A., Abe, A., Bloch, D. R., Eds.; Wiley: New York, 1999; p V/87.
(28) Hasegawa, M.; Kitano, H. *Langmuir* **1992**, *8*, 1582–1586.
(29) Knoner, G.; Rolfe, B. E.; Campbell, J. H.; Parkin, S. J.; Heckenberg, N. R.; Rubinsztein-Dunlop, H. *Biophys. J.* **2006**, *91*, 3085–3096.
(30) Consistent with the literature, we also measured static water contact angles of 88 ± 1° and 60 ± 2° for PS and PMMA, respectively.
(31) Sonka, M.; Hlavac, V.; Boyle, R. *Image Processing, Analysis, and Machine Vision*, 3rd ed.; Cengage Learning: Florence, 2007.
(32) Rasband, W. S. *ImageJ*; U. S. National Institutes of Health: Bethesda, Maryland, 1997−2008; http://rsb.info.nih.gov/ij/.
(33) Knoll, W. *Annu. Rev. Phys. Chem.* **1998**, *49*, 569–638.
(34) Raether, H. *Surface-Plasmons on Smooth and Rough Surfaces and on Gratings*; Springer: Berlin/Heidelberg, 1988; Vol. 111.
(35) Voros, J. *Biophys. J.* **2004**, *87*, 553–561.
(36) Buck, E.; Fuhrmann, J. *Macromolecules* **2001**, *34*, 2172–2178.
(37) Kim, D. H.; Lau, K. H. A.; Robertson, J. W. F.; Lee, O. J.; Jeong, U.; Lee, J. I.; Hawker, C. J.; Russell, T. P.; Kim, J. K.; Knoll, W. *Adv. Mater.* **2005**, *17*, 2442–2446.
(38) Xu, H.; Zhao, X. B.; Grant, C.; Lu, J. R.; Williams, D. E.; Penfold, J. *Langmuir* **2006**, *22*, 6313–6320.
(39) Harris, L. J.; Larson, S. B.; Hasel, K. W.; Day, J.; Greenwood, A.; McPherson, A. *Nature* **1992**, *360*, 369–372.
(40) Kumaki, J.; Hashimoto, T. *J. Am. Chem. Soc.* **2003**, *125*, 4907–4917.
(41) Gunari, N.; Walker, G. C. *Langmuir* **2008**, *24*, 5197–5201.
(42) Ayhan, F.; Rad, A. Y.; Ayhan, H. *J. Biomater. Sci., Polym. Ed.* **2003**, *14*, 1427–1440.
(43) Pratt, W. K. *Digital Image Processing*, 3rd ed.; Wiley-Interscience: New Year, 2001.
(44) Green, P. F.; Limary, R. *Adv. Colloid Interface Sci.* **2001**, *94*, 53–81.
(45) Matsen, M. W. *J. Phys.: Condens. Matter* **2002**, *14*, R21−R47.
(46) Douillard, R.; Daoud, M.; Aguie-Beghin, V. *Curr. Opin. Colloid Interface Sci.* **2003**, *8*, 380–386.
(47) Talbot, J.; Tarjus, G.; Van Tassel, P. R.; Viot, P. *Colloids Surf., A* **2000**, *165*, 287–324.
(48) Lynch, M.; Mosher, C.; Huff, J.; Nettikadan, S.; Johnson, J.; Henderson, E. *Proteomics* **2004**, *4*, 1695–1702.
(49) Raffaini, G.; Ganazzoli, F. *Macromol. Biosci.* **2007**, *7*, 552–566.

BM801158X